Spatial Upper Bound of Radiated Power in Active Antenna Systems

NUSSBAUM Dominique[(1)], RIZK Christ[(1)], SEGUENOT Eric[(1)], KALTENBERGER Florian[(2)],
MORO Andrea[(3)], SINICCO Alessandro[(3)] and POMETCU Laura[(4)]
[(1)]INNOV/ANT Department, ORANGE, Sophia Antipolis, France
[(2)]Communication systems Department, Eurecom, Sophia Antipolis, France
[(3)]Andrew, Agrate Brianza, Italy
[(4)]Agence Nationale des FRequences (ANFR), France

***Abstract*—The assessment of unwanted radiated emissions from Active Antenna Systems (AAS) has become a critical issue in adjacent-band coexistence scenarios. In this paper, we establish the existence of a deterministic spatial upper bound on the radiated power of active antenna arrays. We show that the maximum radiated power always occurs in the boresight direction, irrespective of frequency or signal nature (useful signal, nonlinear distortion, or noise), or instantaneous beamforming configuration, thereby defining a conservative spatial upper bound whose angular envelope is solely determined by the elementary radiating building block of the antenna architecture, i.e., the element or sub-array radiation pattern.**

Starting from a two-element array with third-order nonlinearities, we derive the spatial envelope and extend the result to realistic AAS architectures. The theoretical findings are validated by over-the-air (OTA) measurements performed on a 3.5 GHz Massive Multiple-Input Multiple-Output (MIMO) antenna. The proposed approach offers a simple, robust, and measurement-oriented methodology for coexistence assessments involving beamformed radio systems.

I. Introduction

5G Massive MIMO base stations employ Active Antenna Systems (AAS) with digital beamforming to achieve high spectral efficiency. While enabling sharp in-band directivity, these architectures raise critical questions regarding unwanted radiated emissions in adjacent-band coexistence scenarios, particularly with safety-critical systems like aeronautical radio altimeters. In such contexts, conventional interference assessment approaches, initially devised for passive or weakly directive antennas, may become overly complex or insufficiently conservative when applied to dynamically beamformed AAS.

A. Related work and limitations

Recent work [1] showed that nonlinear distortion of power amplifiers (PA) can remain correlated across antenna branches and be beamformed in the same direction as the intended signal. Our measurements [2] on a 32T32R Massive MIMO radio unit confirmed that spatial directivity of Out-Of-Band (OOB) emissions depends on PA operating regime and Digital Predistortion (DPD) effectiveness.

However, a complementary regulatory question remains: can one establish a simple, conservative bound on maximum radiated emission in any direction, regardless of beamforming configuration, frequency, or signal nature?

B. Contribution and key idea

This paper addresses the above question by establishing that maximum radiated emission always occurs at boresight, defining a deterministic spatial upper bound whose angular envelope is solely determined by the element or sub-array radiation pattern, independent of frequency and signal nature. Starting from a two-element array, we extend the result to realistic AAS and validate it via OTA measurements on a 3.5 GHz Massive MIMO antenna.

C. Methodology and organization

We start from elementary array configurations to provide an intuitive derivation of the spatial envelope, and then extend the reasoning to realistic Massive MIMO AAS architectures.

The remainder of this paper is organized as follows. Section II introduces the two-element reference model. Section III derives the spatial upper bound. Section IV deals with the multi-user transmission, section V extends the result to realistic AAS architectures. Section VI discusses measurement validation and implications. Section VII concludes the paper.

II. Two-Element Array and Third-Order Nonlinearity

A. Two-element array model

We consider the simplest active antenna configuration composed of two identical radiating elements.

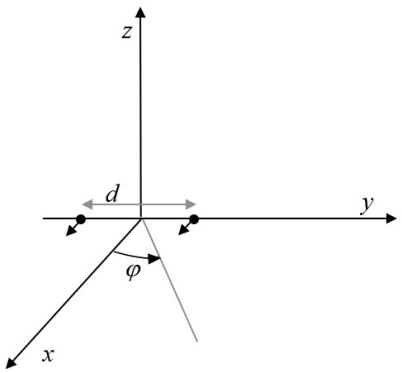

Fig. 1: Two-element array positioned along the y-axis.

The elements are aligned along the y-axis and separated by $d = \lambda/2$, where λ denotes the wavelength at the carrier frequency. This half-wavelength spacing is standard as it avoids grating lobes while maintaining physical compactness. Mutual coupling is neglected, justified for $\lambda/2$ spacing where cross-coupling is typically $< -15\,\text{dB}$ in practical Massive MIMO implementations [3]. Ideal amplitude and phase control is assumed, consistent with modern digital beamforming with calibrated excitation coefficients. The analysis is restricted to the horizontal plane ($\theta = 90°$), the most relevant cut for terrestrial coexistence scenarios, and the azimuth angle $\varphi \in [0, 2\pi]$. The radiation characteristics of the elementary radiator follow the 3GPP antenna modeling framework [4]. The gain in the plane $\theta = 90°$ is given by:

$$A_E(\varphi) = G_{E,\max} + A(\varphi), \tag{1}$$

where $G_{E,\max}$ is the element peak gain and:

$$A(\varphi) = -\min\left\{12\left(\frac{\varphi}{\varphi_{3\text{dB}}}\right)^2, A_m\right\}, \tag{2}$$

where A_m is the front to back ratio and $\varphi_{3\text{dB}}$ is the horizontal half power beamwidth. For a coherent frequency component [3], the radiation pattern of the array in the horizontal plane is expressed as:

$$G(\varphi, \Delta\Phi) = A_E(\varphi) + 20\log_{10}|AF(\varphi, \Delta\Phi)|, \tag{3}$$

where $\Delta\Phi$ denotes the relative excitation phase between the two radiating elements and the array factor in the horizontal plane can be written as:

$$AF(\varphi, \Delta\Phi) = 1 + e^{j(\psi(\varphi)+\Delta\Phi)}, \tag{4}$$

where the geometrical phase term $\psi(\varphi)$ accounts for the propagation path difference between the two elements in the observation direction (φ). For a two-element array with inter-element spacing d and wave number $k = 2\pi/\lambda$, it is given by:

$$\psi(\varphi) = kd\sin\varphi. \tag{5}$$

The magnitude of the array factor is thus:

$$|AF(\varphi, \Delta\Phi)| = 2\left|\cos\left(\frac{\pi d}{\lambda}\sin\varphi + \frac{\Delta\Phi}{2}\right)\right|. \tag{6}$$

B. Spatial Envelope Obtained by Phase Sweeping

We now examine the maximum radiated power that can be obtained in each spatial direction by varying the relative excitation phase $\Delta\Phi$ between the two radiating elements. When the relative phase $\Delta\Phi$ is swept over the full interval $\Delta\Phi \in [0, 2\pi]$, the absolute cosine term spans its entire range, and its maximum value is equal to unity for any φ. Indeed, the absolute cosine function $|\cos(\cdot)|$ is π-periodic. As a consequence, the maximum achievable array factor magnitude in any spatial direction is:

$$\max_{\Delta\Phi}|AF(\varphi, \Delta\Phi)| = 2, \qquad \forall\,\varphi. \tag{7}$$

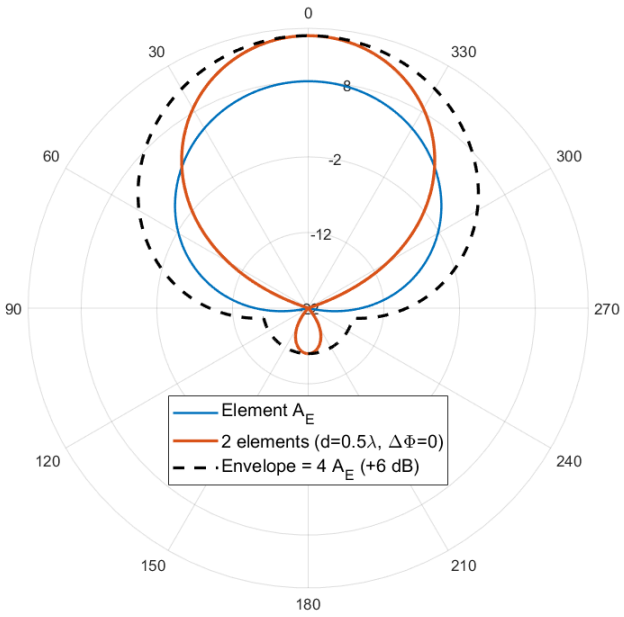

Fig. 2: Two-element array pattern envelope.

It follows that the spatial envelope obtained by sweeping the beamforming phase $\Delta\Phi$ is given by:

$$G_{\text{env}}(\varphi) = A_E(\varphi) + 20\log_{10}(2) = A_E(\varphi) + 6\ \text{dB}. \tag{8}$$

This result shows that, although beamforming allows the main lobe to be steered in any azimuth direction, the maximum radiated power achievable in each direction is fully determined by the element radiation pattern. The spatial envelope is therefore independent of the beamforming phase and is solely governed by the elementary radiator.

III. Spatial Upper Bound of Radiated Power

We now focus on the spatial distribution of radiated power resulting from the two-element array model introduced in Section II. Using the third-order nonlinear signal model, three spectral regions can be identified, depending on the dominant contribution to the radiated signal [2].

Independently of the considered region, we are interested in the maximum radiated power achievable in a given spatial direction when the relative excitation phase $\Delta\Phi$ is swept over its full range $[0, 2\pi]$. This maximum defines a *spatial envelope*, which will be shown to constitute a deterministic upper bound on the radiated power. We first consider a single-user transmission scenario, where the discrete-time complex baseband signal $x(n)$ denotes the useful signal to be transmitted. The signal is assumed to be zero-mean and identical at the input of the two RF chains, up to a controllable excitation phase shift. This single-stream assumption corresponds to the worst-case configuration for radiated power, as all transmit power is concentrated in a single beam; the multi-user case, where power is shared across beams, is addressed in Section IV.

The output of the power amplifier feeding the first radiating element is modeled by a memoryless third-order nonlinearity and can be written as:

$$y_1(n) = x(n) + \alpha|x(n)|^2x(n) + w_1(n), \tag{9}$$

where α denotes the third-order nonlinearity coefficient and $w_1(n)$ is an additive noise term that accounts for thermal noise and residual impairments.

By convention, the second RF chain applies a relative excitation phase $\Delta\Phi$ to the useful signal. The corresponding PA output is therefore given by:

$$y_2(n) = x(n)e^{j\Delta\Phi} + \alpha|x(n)|^2x(n)e^{j\Delta\Phi} + w_2(n), \quad (10)$$

where $w_2(n)$ is assumed to be uncorrelated with $w_1(n)$.

This signal model explicitly separates three contributions at the antenna inputs: the useful in-band component proportional to $x(n)$, the third-order intermodulation (IM) component proportional to $|x(n)|^2x(n)$, and additive noise terms. These three components will be shown to exhibit distinct spatial behaviors, which motivates the identification of three corresponding spectral regions in the following analysis.

A. Useful-signal-dominated region

In the in-band region, the useful signal $x(n)$ dominates. The signals feeding the two radiating elements are phase-shifted versions of the same waveform and therefore remain fully correlated.

As a result, the radiated fields combine coherently. The directional Equivalent Isotropically Radiated Power (EIRP) can be written as:

$$\mathrm{EIRP}_{\mathrm{sig}}(\varphi, \Delta\Phi) = P_e + A_E(\varphi) + 20\log_{10}|AF(\varphi, \Delta\Phi)| \quad (11)$$

where P_e is the conducted power of an element. Sweeping the relative phase $\Delta\Phi$ over $[0, 2\pi]$ yields the spatial envelope:

$$\mathrm{EIRP}_{\mathrm{sig,env}}(\varphi) = P_e + A_E(\varphi) + 6 \text{ dB} \quad (12)$$

The envelope has exactly the same angular shape as the single-element radiation pattern, scaled by a factor four.

B. Third-order-distortion-dominated region

We now consider the adjacent-band region where the third-order distortion term $\alpha|x(n)|^2x(n)$ is predominant. In the present two-element configuration, the input signals applied to the radiating elements differ only by a deterministic phase shift $\Delta\Phi$. The third-order distortion term therefore experiences exactly the same inter-element phase shift as the useful signal. As a consequence, both components share the same array factor and are beamformed in the same spatial direction. The corresponding directional EIRP can be expressed as:

$$\mathrm{EIRP}_{\mathrm{IM3}}(\varphi, \Delta\Phi) = P_{\mathrm{IM3}} + A_E(\varphi) + 20\log_{10}|AF(\varphi, \Delta\Phi)| \quad (13)$$

where P_{IM3} denotes the power of one element associated with the third-order distortion component.

By sweeping $\Delta\Phi$ over $[0, 2\pi]$, the spatial envelope becomes:

$$\mathrm{EIRP}_{\mathrm{IM3,env}}(\varphi) = P_{\mathrm{IM3}} + A_E(\varphi) + 6 \text{ dB} \quad (14)$$

Hence, even in the distortion-dominated region, the maximum radiated power is achieved in the boresight direction and the spatial envelope is again given by the element radiation pattern scaled by a constant factor.

C. Noise-dominated region

Finally, we consider frequency regions where the additive noise terms dominate. In this case, the noise contributions $w_1(n)$ and $w_2(n)$ feeding the two elements are assumed independent and uncorrelated. As a consequence, the radiated powers add incoherently. The resulting directional EIRP is given by:

$$\mathrm{EIRP}_{\mathrm{noise}}(\varphi) = P_{\mathrm{noise}} + A_E(\varphi) + 3 \text{ dB} \quad (15)$$

where P_{noise} denotes the noise power per branch and the +3 dB term accounts for incoherent power addition from two uncorrelated noise sources. Importantly, the spatial distribution of noise does not depend on the relative phase $\Delta\Phi$: for any value of $\Delta\Phi$, the angular shape of the radiated noise power remains identical and follows the single-element radiation pattern. The spatial envelope therefore coincides with this pattern, with a constant $+3$ dB offset.

D. Spatial upper bound

Considering the three spectral regions together, a key conclusion emerges. Regardless of whether the radiated power is dominated by the useful signal, by third-order distortion components, or by noise, the maximum radiated power in any spatial direction is bounded by a deterministic envelope.

Proposition (Two-element case). *For a two-element active antenna array, regardless of beamforming configuration $\Delta\Phi$, signal nature, or frequency, the maximum radiated power in any spatial direction φ is bounded by a deterministic spatial envelope. This envelope has two properties:*

1) *its level is set by the maximum radiated power measured at boresight;*
2) *its angular shape is solely governed by the single-element radiation pattern $A_E(\varphi)$.*

The bound is tight: it is attained at boresight, which is therefore the direction of maximum radiated power for any signal and any beamforming state.

This result establishes the existence of a *spatial upper bound of radiated power*, which is independent of frequency and of the nature of the radiated signal component. It can be naturally generalized with any order of Volterra model. In Section V, this result is extended to realistic AAS architectures to yield the main proposition of this paper.

IV. MULTI-USER TRANSMISSION CASE

We now extend the previous analysis to a multi-user transmission scenario. For clarity, we restrict the discussion to two simultaneously served users, sufficient to highlight the key spatial dispersion mechanisms. The results generalize to $K > 2$ users: the number of distinct cross-IM directions grows combinatorially with K, further increasing spatial dispersion and strengthening the conservativeness of the single-user bound. The memoryless third-order PA model is a simplification; however, as argued in Section III-D, the boresight-maximum property holds for any Volterra order, since it relies solely on phase coherence arguments. Memory effects may alter distortion power levels but do not invalidate the spatial bounding framework.

A. Signal model

Let $u_1(n)$ and $u_2(n)$ denote the discrete-time complex baseband signals associated with user 1 and user 2, respectively. These signals are assumed to be zero-mean and mutually uncorrelated. At the input of the first radiating element, the composite transmit signal is given by the superposition:

$$x_1(n) = u_1(n) + u_2(n). \tag{16}$$

This signal is fed to a power amplifier modeled by a third-order memoryless nonlinearity. The corresponding PA output can be written as:

$$y_1(n) = x_1(n) + \alpha|x_1(n)|^2 x_1(n) + w_1(n), \tag{17}$$

where α denotes the third-order nonlinearity coefficient and $w_1(n)$ is an additive noise term.

For the second radiating element, user-dependent phase shifts are applied in order to form two independent beams. The input signal to the second branch is therefore:

$$x_2(n) = u_1(n)e^{j\Delta\Phi_1} + u_2(n)e^{j\Delta\Phi_2}, \tag{18}$$

where $\Delta\Phi_1$ and $\Delta\Phi_2$ denote the beamforming phase shifts associated with user 1 and user 2, respectively.

After the power amplifier, the output signal of the second branch becomes:

$$y_2(n) = x_2(n) + \alpha|x_2(n)|^2 x_2(n) + w_2(n), \tag{19}$$

where $w_2(n)$ denotes an additive noise term independent of $w_1(n)$. Substituting the beamformed inputs into the PA model, the output signals of the two branches can be written explicitly as For branch 1,

$$\begin{aligned} y_1(n) &= u_1(n) + u_2(n) \\ &\quad + \alpha\Big(|u_1(n)|^2u_1(n) + |u_2(n)|^2u_2(n) \\ &\qquad + |u_1(n)|^2u_2(n) + |u_2(n)|^2u_1(n) \\ &\qquad + u_1^2(n)u_2^*(n) + u_2^2(n)u_1^*(n)\Big) + w_1(n) \end{aligned} \tag{20}$$

For branch 2,

$$\begin{aligned} y_2(n) &= u_1(n)e^{j\Delta\Phi_1} + u_2(n)e^{j\Delta\Phi_2} \\ &\quad + \alpha\Big(\Gamma_{\mathrm{SD}}(n) + \Gamma_{\mathrm{XA}}(n) + \Gamma_{\mathrm{XB}}(n)\Big) + w_2(n), \end{aligned} \tag{21}$$

where $\Gamma_{\mathrm{SD}}(n)$ is the self-distortion:

$$\Gamma_{\mathrm{SD}}(n) = |u_1(n)|^2u_1(n)e^{j\Delta\Phi_1} + |u_2(n)|^2u_2(n)e^{j\Delta\Phi_2} \tag{22}$$

$\Gamma_{\mathrm{XA}}(n)$ is Type-A cross-IM:

$$\Gamma_{\mathrm{XA}}(n) = |u_2(n)|^2u_1(n)e^{j\Delta\Phi_1} + |u_1(n)|^2u_2(n)e^{j\Delta\Phi_2} \tag{23}$$

and $\Gamma_{\mathrm{XB}}(n)$ Type-B cross-IM:

$$\begin{aligned} \Gamma_{\mathrm{XB}}(n) &= u_1^2(n)u_2^*(n)e^{j(2\Delta\Phi_1-\Delta\Phi_2)} \\ &\quad + u_2^2(n)u_1^*(n)e^{j(2\Delta\Phi_2-\Delta\Phi_1)} \end{aligned} \tag{24}$$

The IM components thus fall into three categories. Self-distortion terms ($|u_k|^2u_k$) and Type-A cross-IM terms ($|u_\ell|^2u_k$) both preserve the phase of one user signal and are therefore beamformed in the corresponding user direction. Type-B terms ($u_k^2u_\ell^*$) involve quadratic phase combinations and radiate in additional directions distinct from both user beams. The total distortion power is consequently dispersed over four spatial directions:

1) User 1 direction ($\Delta\Phi_1$): u_1 + self-distortion $|u_1|^2u_1$ + Type-A $|u_2|^2u_1$
2) User 2 direction ($\Delta\Phi_2$): u_2 + self-distortion $|u_2|^2u_2$ + Type-A $|u_1|^2u_2$
3) Cross-IM direction 1 ($2\Delta\Phi_1-\Delta\Phi_2$): Type-B term $u_1^2u_2^*$
4) Cross-IM direction 2 ($2\Delta\Phi_2-\Delta\Phi_1$): Type-B term $u_2^2u_1^*$

From a spatial-power perspective, the multi-user case is intrinsically more favorable than the single-user case for two fundamental reasons. First, **power sharing**: the total transmit power is divided among multiple beams, reducing the peak EIRP in any given direction compared to the single-user boresight configuration. Second, **spatial dispersion of distortion**: third-order IM products spread over four distinct spatial directions, further reducing the radiated power density in any particular direction.

For any given direction φ, the EIRP in the multi-user case therefore satisfies:

$$\mathrm{EIRP}_{\mathrm{MU}}(\varphi) \le \mathrm{EIRP}_{\mathrm{SU,max}}(\varphi), \tag{25}$$

where $\mathrm{EIRP}_{\mathrm{SU,max}}(\varphi)$ denotes the maximum EIRP obtained in the single-user boresight case.

This inequality holds for all the components (useful signal, harmonics and noise). Consequently, the spatial upper bound derived for the single-user case in Section III remains **valid and conservative** in a multi-user transmission scenario. The worst-case radiated power is still achieved in the single-user boresight configuration, and multi-user operation can only reduce the maximum power radiated in any given direction.

V. Extension to Active Antenna Systems and Experimental Validation

In this section, we extend the spatial upper-bound concept derived for the two-element array to a realistic AAS. We then validate the theoretical findings using OTA measurements performed on an antenna previously used in our earlier work [2]. The AAS under test is the SPEAR radio unit from Andrew, and is stimulated by OpenAirInterface (OAI) software [5].

A. Extension of the spatial upper bound to AAS

In a practical AAS, radiating elements are grouped into sub-arrays, each driven by an independent RF chain. Let M denote the number of sub-array rows and N the number of columns. Assuming two orthogonal polarizations ($\pm45°$), the total number of RF chains is equal to $2MN$.

The EIRP in a given direction (θ, φ) is given by [6]:

$$\begin{aligned} \mathrm{EIRP}_{\mathrm{sig}}(\theta,\varphi,\Delta\Phi) &= P_{\mathrm{sub}} + 3\ \mathrm{dB} + A_{\mathrm{sub}}(\theta,\varphi) \\ &\quad + 20\log_{10}|AF_A(\theta,\varphi,\Delta\Phi)| \end{aligned} \tag{26}$$

where P_{sub} is the conducted power of one sub-array, +3 dB accounts for the 2 polarizations, $A_{\mathrm{sub}}(\theta,\varphi)$ is the sub-array radiation pattern, and the array factor is defined as:

$$AF_{\mathrm{A}}(\theta,\varphi) = \sum_{m=0}^{M-1}\sum_{n=0}^{N-1} w_{m,n}\, v_{m,n}(\theta,\varphi) \tag{27}$$

with

$$v_{m,n}(\theta,\varphi) = \exp\left(j2\pi\left[m\frac{d_v}{\lambda}\cos\theta + n\frac{d_h}{\lambda}\sin\theta\,\sin\varphi\right]\right)$$

and

$$w_{m,n} = \exp\left(j\left[m\Delta\Phi_V + n\Delta\Phi_H\right]\right),$$

in which $\Delta\Phi_V$ and $\Delta\Phi_H$ are respectively the relative excitation phase in vertical and horizontal direction. The spatial upper-bound concept derived for the two-element array naturally extends to an AAS. Indeed, for a given observation direction (θ_0,φ_0), the geometrical phase term is fully deterministic. Since the excitation phase gradients $\Delta\Phi_V$ and $\Delta\Phi_H$ are controllable parameters, they can always be selected to compensate the geometrical phase progression. Specifically, choosing:

$$\Delta\Phi_V = -2\pi\frac{d_v}{\lambda}\cos\theta_0, \quad \Delta\Phi_H = -2\pi\frac{d_h}{\lambda}\sin\theta_0\sin\varphi_0$$

yields:

$$m\Delta\Phi_V + n\Delta\Phi_H = -2\pi\left[m\frac{d_v}{\lambda}\cos\theta_0 + n\frac{d_h}{\lambda}\sin\theta_0\sin\varphi_0\right],$$

which exactly cancels the geometrical phase term in $v_{m,n}(\theta_0,\varphi_0)$. Consequently, all phasors in the double summation become co-phased and add constructively. The array factor then reduces to:

$$AF_A(\theta_0,\varphi_0) = MN.$$

Following the reasoning developed in Sections II and III, the elementary radiator in the spatial upper-bound analysis is no longer a single element, but the sub-array itself. Consequently, the spatial envelope governing the maximum radiated power over all beamforming configurations has the angular shape of the sub-array radiation pattern. This result holds for all spectral regions — useful signal, nonlinear distortion of any Volterra order, and noise. This leads to the main result of this paper:

Proposition (Spatial Upper Bound for AAS). *For an Active Antenna System comprising $2MN$ RF chains with two orthogonal polarizations, regardless of beamforming configuration, signal nature, or frequency, the maximum radiated power in any direction (θ,φ) is bounded by a deterministic spatial envelope with two properties:*

1) *its level is set by the maximum radiated power measured at boresight, i.e., $\mathrm{EIRP}_{\mathrm{bound}}(f)$ as defined in (29);*
2) *its angular shape is solely governed by the sub-array radiation pattern $A_{\mathrm{sub}}(\theta,\varphi)$.*

Formally:

$$\mathrm{EIRP}(\theta,\varphi) \le \mathrm{EIRP}_{\mathrm{bound}}(f) + A_{\mathrm{sub}}(\theta,\varphi) - A_{\mathrm{sub}}(\theta_0,\varphi_0), \tag{28}$$

where (θ_0,φ_0) denotes the boresight direction. The bound is tight: it is attained when all $2MN$ sub-arrays are co-phased toward (θ,φ) under single-user transmission. Multi-user operation can only reduce the maximum EIRP in any given direction.

The angular shape of the bound is thus entirely governed by the sub-array radiation pattern, independently of the array size or the beamforming codebook.

B. Measurement setup and frequency-domain characterization

The experimental validation is based on OTA measurements performed in an anechoic chamber using a realistic Massive MIMO antenna operating in the 3.4–3.8 GHz band [2]. The antenna is first configured in a single-user transmission mode with a fixed boresight beam. The received signal is measured in an azimuth cut for $\varphi \in [-60°, 60°]$, using a calibrated probe antenna. The received power spectral density is computed by integrating the received signal power over a bandwidth of 1 MHz. This operation is repeated over the frequency range from 3.4 GHz to 4 GHz, resulting in a spatial and frequency-dependent representation of the Power Spectral Density (PSD). Figure 3 shows the measured boresight PSD for three configurations: full-power 5G NR 100 MHz (3.75 GHz) with DPD, the same signal without DPD, and with 16 dB backoff. Full power corresponds to 72 dBm per polarization (75 dBm total); with a 51 dB path attenuation, the received PSD is approximately 1 dBm/MHz in-band. These curves provide a direct experimental estimate of the maximum radiated power as a function of frequency and serve as a reference upper bound for the angular analysis that follows.

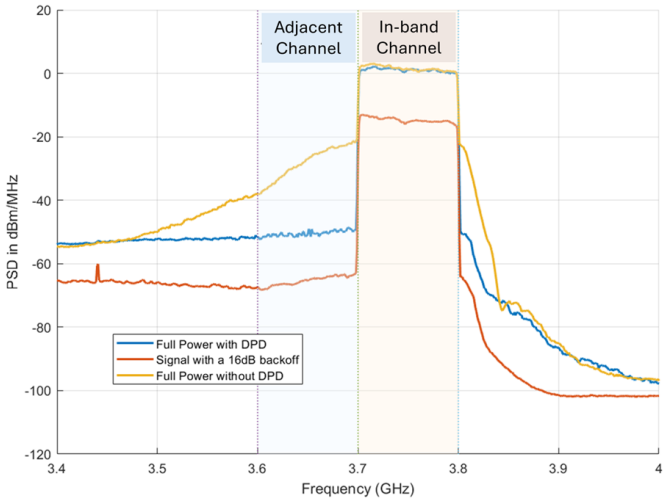

Fig. 3: Measured boresight EIRP spectral density (1 MHz RBW) from 3.4 to 4.0 GHz for three configurations (Full power with and without DPD, 16 dB backoff). Vertical dashed lines indicate measurement frequencies for angular analysis: 3.75 GHz (in-band region), 3.65 GHz (IM3 and noise dominated region).

Figure 4 shows the angular distribution of radiated power for the boresight beam configuration, normalized to 0 dB at boresight. This normalization removes absolute power levels and isolates the spatial shape of each spectral component. The adjacent-channel pattern without DPD closely follows the in-band shape, confirming that IM products are beamformed in the same spatial direction as the useful signal. With DPD or 16 dB backoff, IM levels drop substantially and the adjacent-band distribution spreads spatially, approaching the wider shape of the sub-array envelope.

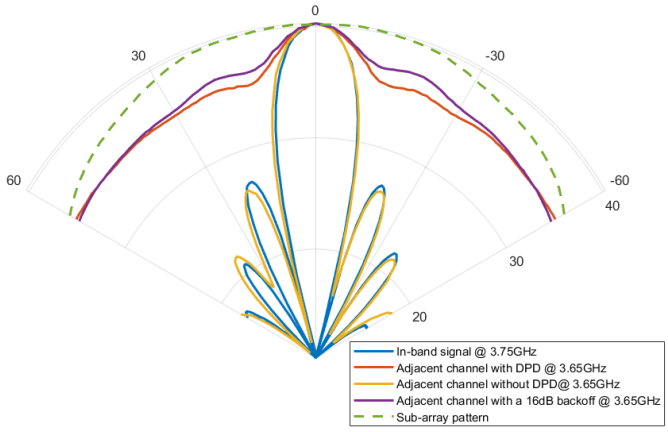

Fig. 4: Spatial distribution of radiated power for a fixed boresight beam, integrated over 100 MHz, for four spectral configurations: in-band signal (3.75 GHz), adjacent channel without DPD (3.65 GHz), adjacent channel with DPD, and adjacent channel with 16 dB backoff. All patterns are normalized to their boresight level (0 dB reference), so that only the angular shape of each distribution is compared, independently of absolute power levels. The normalization highlights how the spatial concentration of OOB emissions varies with DPD state and operating point.

In a second experiment, radiation patterns are measured for various beam directions ($-42°$, $-30°$, $-18°$, $0°$, $18°$, $30°$ and $42°$), using full power signal with DPD. The boresight EIRP measurement serves as the reference level for the spatial bound. According to 3GPP TS 38.141-2 (Release 18), the OTA uncertainty for FR1 measurements in the range $3\,\text{GHz} < f \leq 7.125\,\text{GHz}$ is $\pm 1.3\,\text{dB}$ (95% confidence). A conservative one-sided bound is therefore defined as

$$\text{EIRP}_{\text{bound}}(f) = \text{EIRP}_{\text{meas}}(f) + 1.3\,\text{dB}. \tag{29}$$

For OOB and spurious quantities, uncertainties may reach up to 3 dB. Sub-array pattern measurements are subject to the same uncertainty; manufacturing dispersion between sub-arrays introduces additional angular-dependent deviations, addressable through worst-case characterization or a statistically derived margin. Figure 5 shows the radiation patterns (azimuth cuts) of the in-band [Fig. 5(a)] and adjacent spectral components [Fig. 5(b)] for various beam directions, together with the theoretical spatial upper bound derived from the boresight level via (29), and the shape of a theoretical sub-array following the 3GPP antenna modeling framework [4] with $\varphi_{3\text{dB}} = 85°$.

An excellent agreement is observed between the theoretical bound and the measured radiation levels across all beam steering configurations. Quantitatively, the maximum deviation between the theoretical spatial envelope and measured EIRP is less than 1 dB for all seven beam directions in both spectral regions (in-band and adjacent band). This remarkable agreement validates three key aspects of the proposed framework:

1) The spatial upper bound derived from boresight measurement accurately predicts the maximum EIRP envelope for arbitrary beam steering directions.
2) The 3GPP sub-array radiation pattern model ($\varphi_{3\text{dB}} = 85°$, $A_m = 30\,\text{dB}$) provides an accurate representation of the elementary radiator characteristics of the antenna under test.
3) The theoretical prediction that maximum radiated emission always occurs at boresight holds regardless of beam steering angle.

(a) In-band (3.75 GHz)

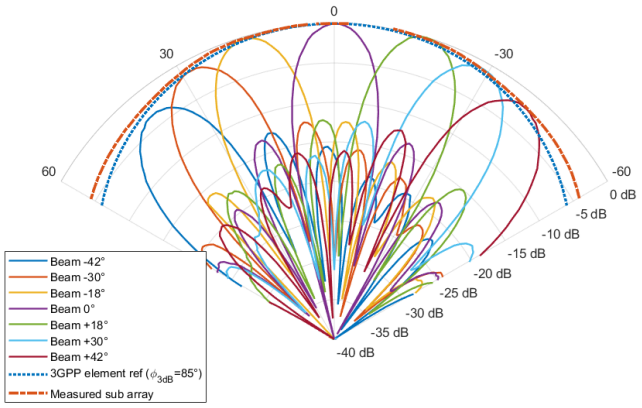

(b) Adjacent band (3.65 GHz)

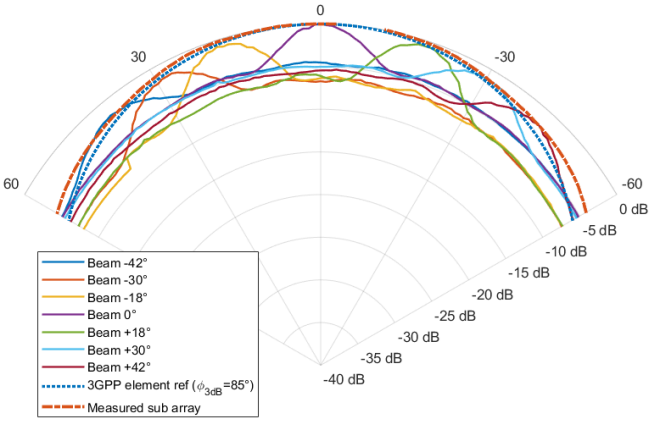

Fig. 5: Validation of the spatial upper bound for seven beam steering angles ($-42°$, $-30°$, $-18°$, $0°$, $18°$, $30°$, $42°$). **(a)** In-band and **(b)** adjacent-band radiation patterns. Solid colored lines: measured EIRP per beam direction. Dotted line: 3GPP sub-array element reference ($\varphi_{3\text{dB}} = 85°$). Dash-dot line: measured sub-array pattern (spatial upper bound). All patterns normalized to boresight (0 dB).

Concerning the adjacent band, the signal (with DPD) is a mixture of residual IM components and noise. The sub-1 dB margin between theory and measurement is well within the expected OTA uncertainty (± 1.3 dB for in-band, ± 3.0 dB for out-of-band per 3GPP TS 38.141-2), confirming the conservativeness and practical applicability of the proposed spatial upper bound framework.

C. Experimental Validation in the Multi-User MIMO Case

We now verify experimentally the analytical predictions of Section IV. The multi-user (MU) scenario was experimentally evaluated using the antenna configured to simultaneously serve two users steered toward distinct azimuth directions. The users were pointed toward $\varphi_1 = 0°$ and $\varphi_2 = 18°$.

For each azimuth angle, the radiated power was computed by integrating the PSD over the in-band and adjacent band. Measurements were performed with and without DPD in order to clearly observe the spatial components of the adjacent band. According to the model used in Section IV, the nonlinear output of each branch contains:

1) Self-distortion terms and Type A cross-IM, proportional to $|u_k|^2 u_k$ and $|u_\ell|^2 u_k$, which preserve the phase gradient of one of the users and therefore radiate in the original user directions φ_1 and φ_2.
2) Type B cross-IM terms, proportional to $u_1^2 u_2^*$ and $u_2^2 u_1^*$, which generate additional phase gradients:

$$\Delta\Phi_{B1} = 2\Delta\Phi_1 - \Delta\Phi_2, \qquad \Delta\Phi_{B2} = 2\Delta\Phi_2 - \Delta\Phi_1. \tag{30}$$

For an AAS steered in azimuth, where the phase gradient satisfies $\Delta\Phi(\varphi) \propto \sin\varphi$, the corresponding directions are:

$$\sin\varphi_{B1} = 2\sin\varphi_1 - \sin\varphi_2, \qquad \sin\varphi_{B2} = 2\sin\varphi_2 - \sin\varphi_1. \tag{31}$$

For $\varphi_1 = 0°$ and $\varphi_2 = 18°$, this yields:

$$\varphi_{B1} \approx -18°, \qquad \varphi_{B2} \approx 38.2°. \tag{32}$$

Therefore, in addition to the two useful beams, two additional spatial directions are theoretically expected for third-order IM products. Figure 6 shows the angular distribution of

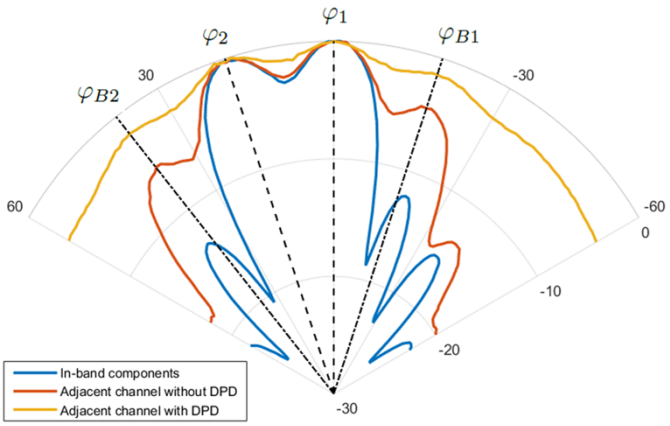

Fig. 6: Spatial distribution of radiated power in the multi-user configuration with two users steered at $\varphi_1 = 0°$ and $\varphi_2 = 18°$, for three spectral components: in-band (3.75 GHz), adjacent channel without DPD (3.65 GHz), and adjacent channel with DPD. All patterns are normalized to their boresight level (0 dB reference), so that only the angular shape of each distribution is compared, independently of absolute power levels. Dashed lines indicate the predicted directions: φ_1, φ_2 for the user beams, and $\varphi_{B1} \approx -18°$, $\varphi_{B2} \approx 38.2°$ for the Type-B cross-IM products.

radiated power for the multi-user configuration. All patterns are normalized to their boresight level (0 dB reference), so that the figure displays only the spatial shape of each distribution, independently of absolute power levels. The in-band radiation exhibits two main lobes aligned with the user directions (0° and 18°), as expected from the beamforming configuration. The adjacent-band distribution without DPD shows a clear angular structure with maxima partially aligned with the user beams, consistent with the Type A distortion terms, and evidence of additional spreading toward the predicted Type B directions. With DPD, this spatial spreading is mitigated.

These experimental observations validate the analytical framework developed in Section IV. In particular, they confirm that:

- third-order nonlinear products in MU transmission generate additional spatial components,
- the spatial distribution of OOB radiation is inherently more dispersed in MU compared to the single-user case.

VI. Discussion and Implications for Coexistence

This work does not aim at defining a normative 3GPP-compliant limit. Instead, it proposes a conservative engineering framework to derive a spatial upper bound from boresight measurements for coexistence analyses. The proposed bound has three key implications for coexistence assessments involving AAS.

A. Independence from correlation modeling

The spatial upper bound does not require explicit knowledge of the spatial correlation between RF chains. It is fully characterized by: (i) the maximum power spectral density measured in the boresight direction, and (ii) a deterministic spatial envelope governed by the elementary radiator (element or sub-array).

Correlation effects, often quantified by a factor ρ [6], mainly affect the degree to which unwanted emissions are beamformed. However, this influence is implicitly captured in the measured boresight spectrum. When nonlinear distortion increases, the adjacent-channel leakage ratio (ACLR) degrades, and any degradation due to correlated distortion components is reflected uniformly in the spatial envelope, which bounds the radiated emissions in all directions. As a consequence, the upper bound remains valid and conservative without requiring explicit modeling of distortion correlation mechanisms.

B. Role of DPD

DPD plays a dual role. First, it reduces unwanted signals in conducted mode by improving ACLR. Second, by suppressing correlated distortion components, it limits their coherent beamforming in the radiated domain. When distortion becomes noise-like, emissions add predominantly incoherently, resulting in a flatter spatial distribution. Hence, DPD reduces both the absolute emission level and its spatial concentration. This dual effect highlights the central role of DPD in modern Massive MIMO transmitters, not only for in-band linearity but also for spatial control of out-of-band emissions.

C. Practical workflow for coexistence assessments

From a regulatory and system-engineering perspective, the main benefit of the proposed framework is methodological simplification. Rather than modeling detailed beamforming states or nonlinear distortion mechanisms, a conservative upper bound can be derived directly from boresight measurements at maximum transmit power.

The practical workflow for applying this bound in a coexistence study can be summarized as follows:

1) **Boresight EIRP measurement:** Measure $\mathrm{EIRP}_{\mathrm{meas}}(f)$ at boresight under maximum transmit power, using a single well-defined beam. This requires only standard OTA instrumentation, independent of the beamforming codebook.
2) **Uncertainty margin:** Apply the margin per (29) ($+1.3\,$dB in-band, $+3\,$dB for OOB per 3GPP TS 38.141-2) to obtain $\mathrm{EIRP}_{\mathrm{bound}}(f)$.
3) **Sub-array pattern:** Determine $A_{\mathrm{sub}}(\theta, \varphi)$ by measurement or via the 3GPP model [4]. This defines the angular shape of the bound.
4) **Spatial bound computation:** For any direction (θ, φ) and frequency f:

$$\mathrm{EIRP}_{\mathrm{UB}}(\theta, \varphi, f) = \mathrm{EIRP}_{\mathrm{bound}}(f) + A_{\mathrm{sub}}(\theta, \varphi) - A_{\mathrm{sub}}(\theta_0, \varphi_0),$$

where (θ_0, φ_0) denotes the boresight direction, consistent with the notation of Proposition V-A.

This measurement-oriented approach preserves physical rigor while substantially reducing the complexity of interference assessments. It is particularly suited for regulatory type-approval testing, where reproducibility and conservatism are prioritized over simulation fidelity.

D. Limitations and scope of applicability

While the proposed framework has been shown to be robust across spectral regions and beam steering angles, several limitations should be acknowledged when considering its application to other scenarios.

Array architecture and mutual coupling: The derivation assumes that all sub-arrays share a common elementary radiation pattern and that the array factor model of (27) applies, which requires uniform sub-array groupings and low inter-element coupling. This is justified for $\lambda/2$ spacing, where cross-coupling is typically $< -15\,$dB in practical Massive MIMO implementations. For non-uniform sub-array groupings, or for compact or irregular geometries where mutual coupling becomes significant (typically above $-10\,$dB), the sub-array pattern may be distorted and the spatial envelope may deviate from the model.

PA nonlinearity model: The spatial upper-bound result is structurally valid for nonlinear models of arbitrary Volterra order, as the boresight-maximum property relies solely on phase-coherence arguments that are independent of the polynomial order. The main limitation is the absence of memory effects in the PA model: frequency-dependent nonlinearities, which may be significant at high modulation bandwidths, are not captured. Accounting for such effects is left for future work.

Angular coverage: The experimental validation was performed in the azimuth plane ($\theta = 90°$). Extension to full 3D radiation patterns, including elevation-plane steering and cross-polarization effects, is conceptually straightforward within the proposed framework but has not been validated experimentally.

VII. Conclusion

This paper established a deterministic spatial upper bound for the radiated power of beamforming AAS. Starting from a two-element array with third-order nonlinearities, we showed that the spatial envelope coincides with the elementary radiator pattern and reaches its maximum at boresight. This preliminary result was then generalized to yield the main contribution: a formal spatial upper bound for any AAS with $2MN$ RF chains (Proposition V-A, (28)), valid regardless of array size, beamforming configuration, signal nature, frequency, or RF-chain correlation. The bound is fully characterized by the measured boresight EIRP and the sub-array radiation pattern, and is tight under single-user boresight transmission.

Experimental validation on a 3.5 GHz Massive MIMO antenna confirmed the predictions across three spectral regions and seven beam steering angles, with deviations below OTA measurement uncertainty. A practical workflow for applying the bound in regulatory coexistence assessments was proposed, requiring only boresight OTA measurements and sub-array pattern characterization. The framework is structurally valid for higher-order Volterra PA models; limitations regarding non-uniform sub-array groupings, strong mutual coupling, PA memory effects, and 3D angular coverage were identified as directions for future work.

References

[1] E. G. Larsson and L. Van der Perre, "Out-of-Band Radiation From Antenna Arrays Clarified," *IEEE Wireless Communications Letters*, vol. 7, no. 4, pp. 610–613, Aug. 2018.

[2] C. Rizk, D. Nussbaum, E. Seguenot, F. Kaltenberger, A. Moro, and A. Sinicco, "Actual Out-of-Band Emissions from Massive MIMO Antennas," EURECOM, Sophia Antipolis, France, Tech. Rep., Oct. 2025, presented Feb. 2026. [Online]. Available: https://www.eurecom.fr/en/publication/8396

[3] C. A. Balanis, *Antenna Theory: Analysis and Design*, 4th ed. Hoboken, NJ, USA: Wiley, 2016.

[4] 3GPP, "Study on New Radio (NR) Access Technology – RF and Coexistence Aspects," 3rd Generation Partnership Project, Technical Report TR 38.803, 2024, release 14. [Online]. Available: https://www.3gpp.org

[5] F. Kaltenberger, T. Melodia, I. Ghauri, M. Polese, R. Knopp, T. T. Nguyen, S. Velumani, D. Villa, L. Bonati, R. Schmidt, S. Arora, M. Irazabal, and N. Nikaein, "Driving Innovation in 6G Wireless Technologies: The OpenAirInterface Approach," *Computer Networks*, vol. 269, p. 111410, Sep. 2025.

[6] 3GPP, "Study on International Mobile Telecommunications (IMT) Parameters," 3rd Generation Partnership Project, Technical Report TR 38.922, 2025, release 19. [Online]. Available: https://www.3gpp.org

[7] R. C. Hansen, *Phased Array Antennas*. Wiley, 2009.